BRNO UNIVERSITY OF TECHNOLOGY

VYSOKÉ UČENÍ TECHNICKÉ V BRNĚ

FACULTY OF MECHANICAL ENGINEERING

FAKULTA STROJNÍHO INŽENÝRSTVÍ

INSTITUTE OF MANUFACTURING TECHNOLOGY

ÚSTAV STROJÍRENSKÉ TECHNOLOGIE

OPTIMISATION OF MOTORCYCLE FRAME FROM COMPOSITE MATERIALS CONSIDERING MANUFACTURING TECHNOLOGY

OPTIMALIZACE KONSTRUKCE MOTOCYKLOVÉHO RÁMU Z KOMPOZITNÍCH MATERIÁLŮ S OHLEDEM NA VÝROBNÍ TECHNOLOGII

THESIS STATEMENT

TEZE

AUTHOR Ing. Lukáš Gregor

AUTOR PRÁCE

SUPERVISOR doc. Ing. Jan Zouhar Ph.D.

ŠKOLITEL

BRNO 2025

KEYWORDS

CFRP, topological optimisation, motorcycle, simulation, FEM, composite, frame

CONTENT

INTRODUCTION

The automobile is a revolutionary invention that fundamentally transformed ground transportation. The potential of this transformation lay in the possibility of transporting people and goods almost independently and at high speed to virtually any destination, according to individual needs. This gave rise to one of the most widespread industrial sectors, which, alongside aviation and astronautics, has significantly contributed to the advancement of mechanical engineering technologies. The motorcycle, originally developed as a more affordable alternative to the automobile, today finds application primarily due to its compactness in countries with high population density. Alternatively, it serves as a leisure or sports vehicle, owing to its favourable power-to-weight ratio. Similar to the automotive sector, the motorcycle industry is also experiencing, albeit with some delay, the trend of electrification.

Electric motorcycles offer a number of undeniable advantages. Their main benefit lies in the simplicity of the power unit design, which allows for new approaches to layout, integration, and ergonomics. Examples include the composite motorcycle frame of the Novus (Fig. 1) and the forged aluminium frame of the Cake Bukk (Fig. 2). From a performance and handling perspective, electric drive enables more precise modulation of power delivery to the wheel, while torque output depends solely on motor speed and the controller input. The primary drawback is the issue of limited range and charging times, both determined by battery capacity. This, however, is generally less critical than in the case of passenger electric cars, since apart from touring motorcycles long range is not usually a requirement [1]. Statistical data on motorcycle use in England show that approximately 55 % of all rides are commuting trips, with an average ride length of 18 km. Only around 10 % of trips involve full-day or long-distance travel, where range limitations could become problematic [2].

A critical disadvantage of electric motorcycles arises in the comparison between the time needed to refuel a gasoline tank and the time required to recharge a battery of equivalent energy capacity, where the difference may reach two orders of magnitude. Moreover, the specific energy density of current lithium-ion batteries remains low, at approximately 250 Wh kg^{-1}, which is about fifty times less than that of gasoline (12,700 Wh kg^{-1}). This significantly increases vehicle mass as a function of battery size. A potential solution would be the industrial-scale deployment of lithium–sulfur batteries (2,600 Wh kg^{-1}) or even lithium–air batteries (11,140 Wh kg^{-1}), although at present these technologies are only applicable under laboratory conditions (see e.g. [3–5]). An alternative approach to addressing this limitation is motorcycle hybridization. A small battery combined with an internal combustion engine operating only in eco-driving modes or at low states of charge could preserve low mass while extending range [6]. Furthermore, with the utilization of green fuels [7] and the current global energy mix [8] such a solution could represent an environmentally friendly drive concept.

However, the implications of larger battery capacity namely higher weight and higher energy consumption suggest that, within the context of the energy source, electric motorcycles may not necessarily represent a more ecological option over their entire life cycle (see e.g.[1, 9, 10]). Consequently, weight minimization, as a critical parameter in the transportation sector, should remain a design priority even in the era of electrification. One promising method of weight reduction lies in the application of advanced composite materials, particularly carbon-fibre reinforced polymers (CFRP), in the design of structural components. The potential of such materials for effective weight reduction is demonstrated in the aviation industry, where the use of composites enabled a 20 % mass saving in the Boeing 787 airliner [11]. Another undeniable advantage of composites is their excellent resistance to corrosion and fatigue, both of which are of significant importance in motorcycle applications (see e.g. [12–14]).

For these reasons, this dissertation addresses the application of modern optimisation technique topology optimisation (TO) to improve existing structural solutions and rationalize the design and manufacturing of a carbon-fibre reinforced motorcycle frame. The aim is to achieve weight reduction while ensuring the required structural stiffness and sufficient safety.

Fig. 1 Novus motorcycle with a composite frame [15]

Fig. 2 Cake Bukk motorcycle with a forged aluminium frame [16]

1 AIM OF THE THESIS

The main aim of this dissertation is to verify the methodology of applying topology optimisation to the design of structural composite components. The primary motivation arises from the fact that this method remains insufficiently explored and rarely applied, mainly due to manufacturing constraints and a limited understanding of its potential.

The specific objectives of the thesis are as follows:

- To compare the structural stiffness and strength of the existing composite frame with the properties achievable through topology-driven geometry modifications, while maintaining the same laminate lay-up and identical input conditions.
- To demonstrate how topology optimisation can serve as a supporting tool for the design of manufacturable composite structures without altering the principal material composition.

2 STATE OF THE ART

2.1 TOPOLOGY OPTIMISATION IN COMPOSITES

The application of topology optimisation to composite materials is more challenging than for isotropic metals due to their anisotropic behaviour. Simplified two-dimensional approaches, for example beam models, have demonstrated significant potential. Hu [36, 37] showed that the use of topology optimisation can reduce deformation by up to 20% compared to conventional lightweight design methods. Zhang [17] further demonstrated that aligning fibres along principal stress trajectories in combination with topology optimisation can increase beam modulus by 40% and improve the stiffness-to-weight ratio by 35%. Chen [18] reported stiffness improvements exceeding 1000% for 3D-printed carbon-fibre reinforced polyamide when applying topology optimisation compared to the neat polymer.

Further advances have been achieved through tailored fibre placement (TFP), where fibres are deposited along calculated load paths. This approach was experimentally validated by Schwingel [19] and Spickenheuer [20], while Coppola [21] successfully manufactured a connecting rod using this method. A similar potential is seen in additive manufacturing of continuous fibre composites, demonstrated by Suzuki [22].

Although no publication has yet reported the direct application of topology optimisation to the design of three-dimensional composite shells or bonded assemblies, the study by Kdovin [23] demonstrates its potential. In this work, topology optimisation was employed to propose an optimal mass distribution, which was subsequently realised as a welded tubular frame. The resulting structure exhibited an increase of 250% in longitudinal and torsional stiffness, while simultaneously achieving a 15% weight reduction. Although the outcome was not a composite shell, this example illustrates the capability of topology optimisation to generate efficient load paths, and a similar concept could be applied to the design of composite monocoque structures.

2.2 DESIGN REQUIREMENTS FOR A MOTORCYCLE FRAME

The motorcycle frame represents the primary structural element of the vehicle and must therefore satisfy a complex set of requirements. These requirements can be divided into several categories:

- Structural stiffness, which determines the handling characteristics and stability of the motorcycle under dynamic loading. The most important parameters are torsional, longitudinal, and lateral stiffness.
- Strength under specific loading conditions, ensuring the durability of the structure during braking, cornering, and landing after jumps.
- Integration of auxiliary systems, including the installation and protection of the battery pack, the mounting of the power unit, the fuel tank, and the bodywork. These components impose additional constraints on the frame geometry, load-bearing capacity, and accessibility.

2.3 ANALYSIS OF THE BASELINE DESIGN

A motorcycle frame is generally defined as the structural element that supports the engine, incorporates the steering head, and provides the mounting points for the rear swingarm [24]. In the proposed design concept, the frame is divided into two parts. The composite section, designed as a monocoque – that is, a shell-type structure carrying loads through its continuous skin rather than through discrete members – functions simultaneously as an airbox for the combustion engine, a housing for the battery modules, and the support for the steering head, while transferring loads into the aluminium section of the frame, represented by the crankcase. The aluminium part accommodates the power unit and provides the pivot connection for the rear swingarm. The division of the frame into its composite and aluminium sections is illustrated in Fig. 3.

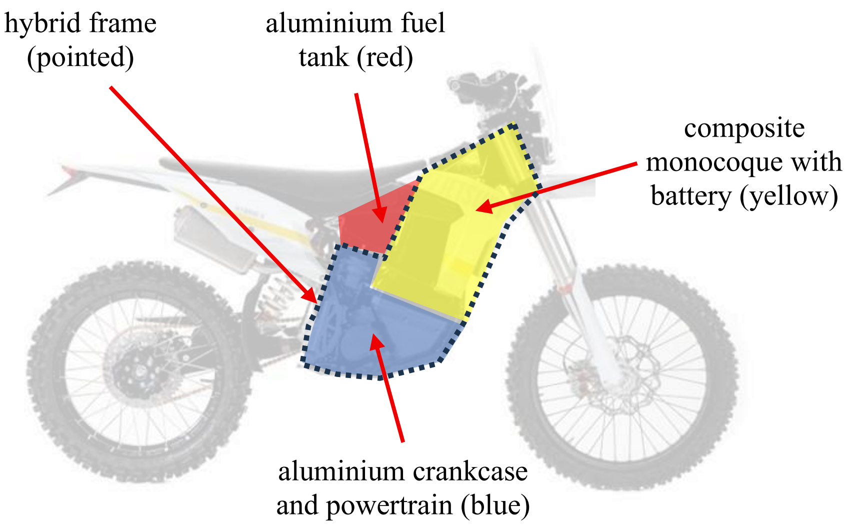

Fig. 3 Division of the hybrid motorcycle frame

2.3.1 DESIGN CONSTRAINTS

The overall spatial layout of the frame is primarily determined by a set of design constraints. These include rider ergonomics, positioning of the steering head, integration of battery modules into the monocoque, and dimensional requirements arising from the installation of other components such as the electric motor, combustion engine, control unit, fuel tank, and airbox. In addition, aesthetic and stylistic considerations also play a role in the design of the frame.

RIDER ERGONOMICS

One of the most critical criteria for defining geometric constraints is rider ergonomics. The motorcycle must remain user-friendly and comfortable across a broad range of potential riders. Within the CAD environment, an ergonomic digital human model representing the 50th percentile male was used as the baseline reference for defining key geometric parameters such as seating position, leg angles, monocoque width, and the placement of control elements (foot pegs, handlebars, etc.). The positions of the 50th percentile male used for these evaluations are illustrated in Fig. 4.

To verify the suitability of the design for the wider rider population, additional checks were performed with the 5th percentile male and the 95th percentile male, ensuring that the geometry remains acceptable for both smaller and taller riders. The proposed geometry was continuously validated against real motorcycles of comparable category through iterative ergonomic verification. An overview of rider stature is given in Tab. 1, where only height values are listed; all other anthropometric data are available in the literature [25].

Tab. 1 Basic anthropometric data [25]

Percentile	5th	50th	95th
Approx. height	168 cm	175 cm	188 cm

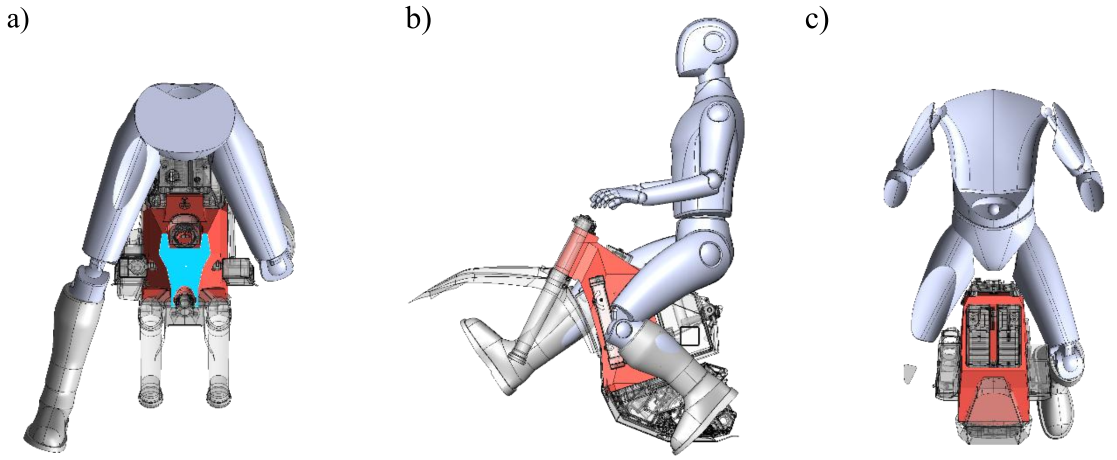

Fig. 4 Ergonomic model (50th percentile) positioning with foot on the footrest and extended leg during cornering: a) top view showing rider leg angle relative to monocoque and radiator, b) side view of rider posture, c) vertical section showing leg position relative to monocoque and radiator

STEERING HEAD

Another key design constraint is the positioning of the steering head, which determines the neck width of the monocoque and simultaneously limits the maximum handlebar rotation angle. In the proposed concept, this angle was set to 45°. For comparison, enduro motorcycles typically allow 45–55°, while city motorcycles and scooters usually provide 35–45°. The selected value of 45° therefore lies at the lower boundary of the typical enduro range, while fully corresponding to city motorcycles [26, 27].

RAKE ANGLE

The hybrid powertrain concept and the associated aluminium–composite frame were designed to reduce production costs and broaden customer appeal by enabling applicability to both enduro and city motorcycles. These two categories, however, differ in their steering head angle (rake angle). For city motorcycles, typical rake values are in the range of 24–26°, with the baseline concept set to 25°. Enduro motorcycles usually employ values around 26–28°, with the proposed design adopting 26.5°. These differences reflect the distinct requirements for manoeuvrability and stability in the two categories. The composite monocoque was therefore designed to accommodate both configurations with only minor modifications, achieved primarily through variations in the positioning of bonded aluminium inserts for the fork mounting.

FRONT SUSPENSION TRAVEL

Front suspension travel constitutes an additional boundary condition that must be respected in the design of the motorcycle frame. As the front fork compresses, the wheel follows a defined path which requires sufficient clearance from the frame structure. This kinematic constraint limits the available design space in the steering head region and must therefore be taken into account during the definition of the structural geometry, as illustrated in Fig. 5.

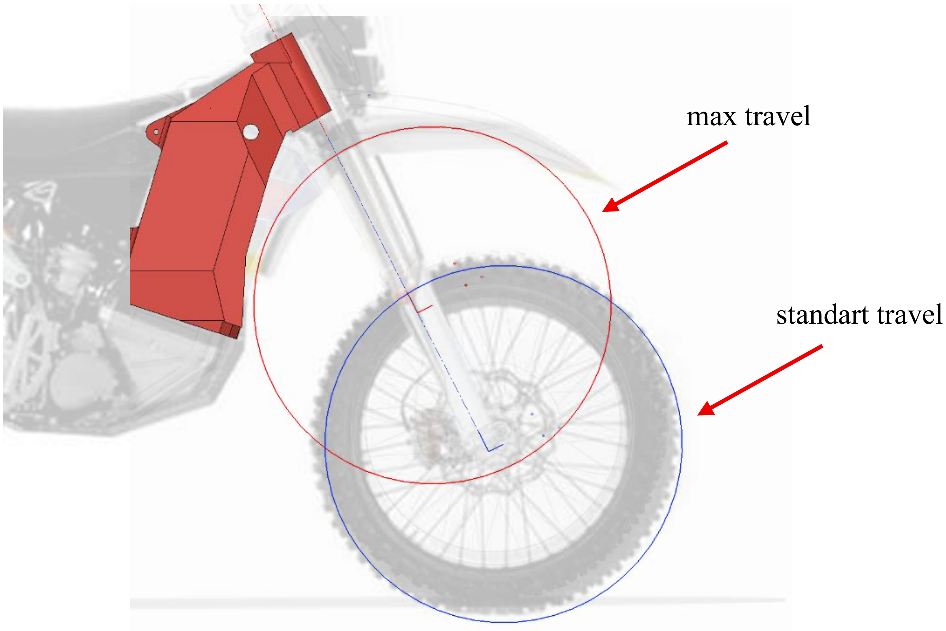

Fig. 5 Maximum front suspension travel

INTEGRATION OF BATTERY SYSTEM

A major design constraint is the integration of the battery system. Since the battery modules are based on an existing prototype, the monocoque geometry was adapted accordingly (Fig. 6). The structure must also enable the removal of modules if required and provide sufficient space for partial passive air cooling, even though the composite casing primarily acts as a thermal insulator. In addition, the monocoque fulfils a dual role as an airbox for the combustion engine. It therefore incorporates a plenum chamber with integrated filtration, designed for the requirements of a 100 cm³ single-cylinder two-stroke engine. For optimal performance, an airbox volume of 8–12 dm³ is recommended to stabilise intake pulsations, ensure reliable cylinder charging, and attenuate intake noise.

FUEL TANK AND CRANKCASE

Another key geometric constraint arises from the positioning of the fuel tank and the crankcase. The fuel tank, with a predefined volume, is mounted above the monocoque and secured by two pins. The engine is housed within a crankcase derived from an existing prototype, which imposes further restrictions on the frame concept. To ensure reliable integration, the interface incorporates bonded flanges for joining the monocoque with the crankcase and inserts for securely connecting the fuel tank. The locations of these flanges and fuel tank inserts are shown in Fig. 6.

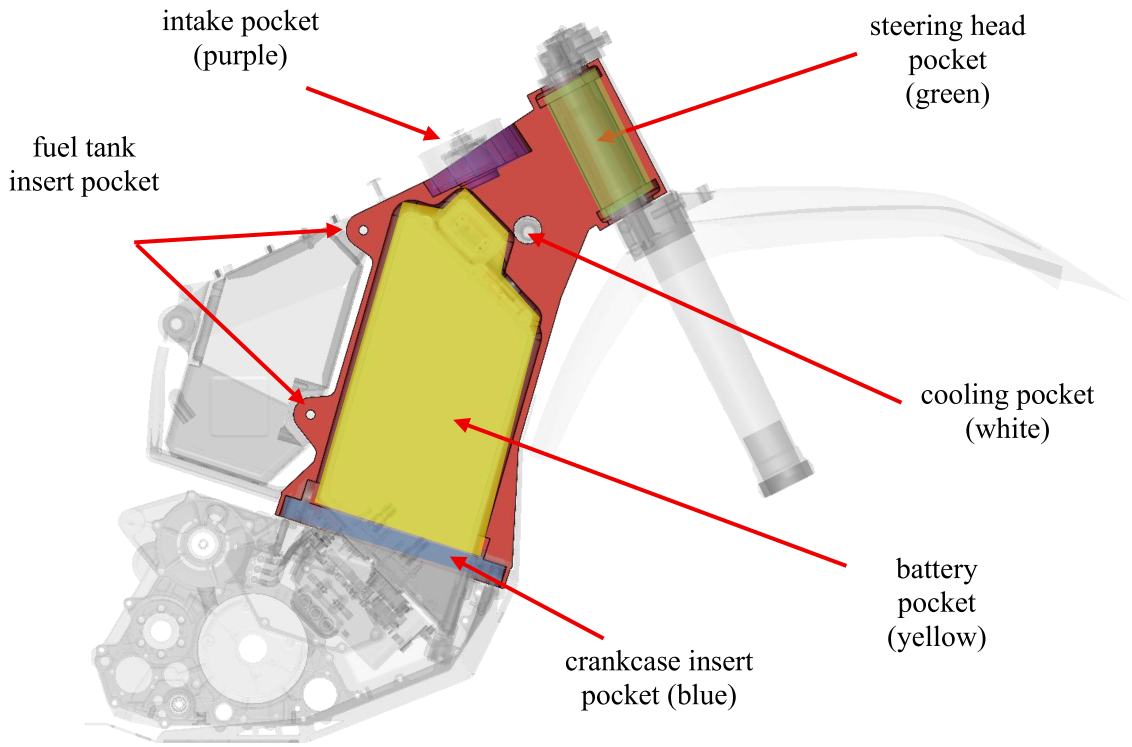

Fig. 6 Design constraints from integrated components

COOLING HOSE ROUTING

A specific constraint is the routing of cooling hoses connecting the radiators mounted on both sides of the motorcycle. These hoses must pass directly through the monocoque, which therefore requires defined channels or openings to ensure safe passage. Adequate clearance between the hoses and the structural walls must also be maintained, both for mechanical protection and to minimise vibration transfer.

2.3.2 DEFINITION OF THE BASELINE DESIGN

Based on the above geometric and design constraints, the monocoque frame was constructed as a bonded composite shell assembled from multiple composite and aluminium parts (Fig. 7). This version represents a pragmatic compromise, created to accelerate development by following the preliminary visual design prepared by an industrial designer. It was conceived primarily on an empirical basis, without the use of advanced computational optimisation tools. The objective at this stage was to validate the hybrid motorcycle concept, with subsequent optimisation of layup sequences and structural performance planned as future work. Validation was intended through both mechanical testing of structural components and full-scale riding tests.

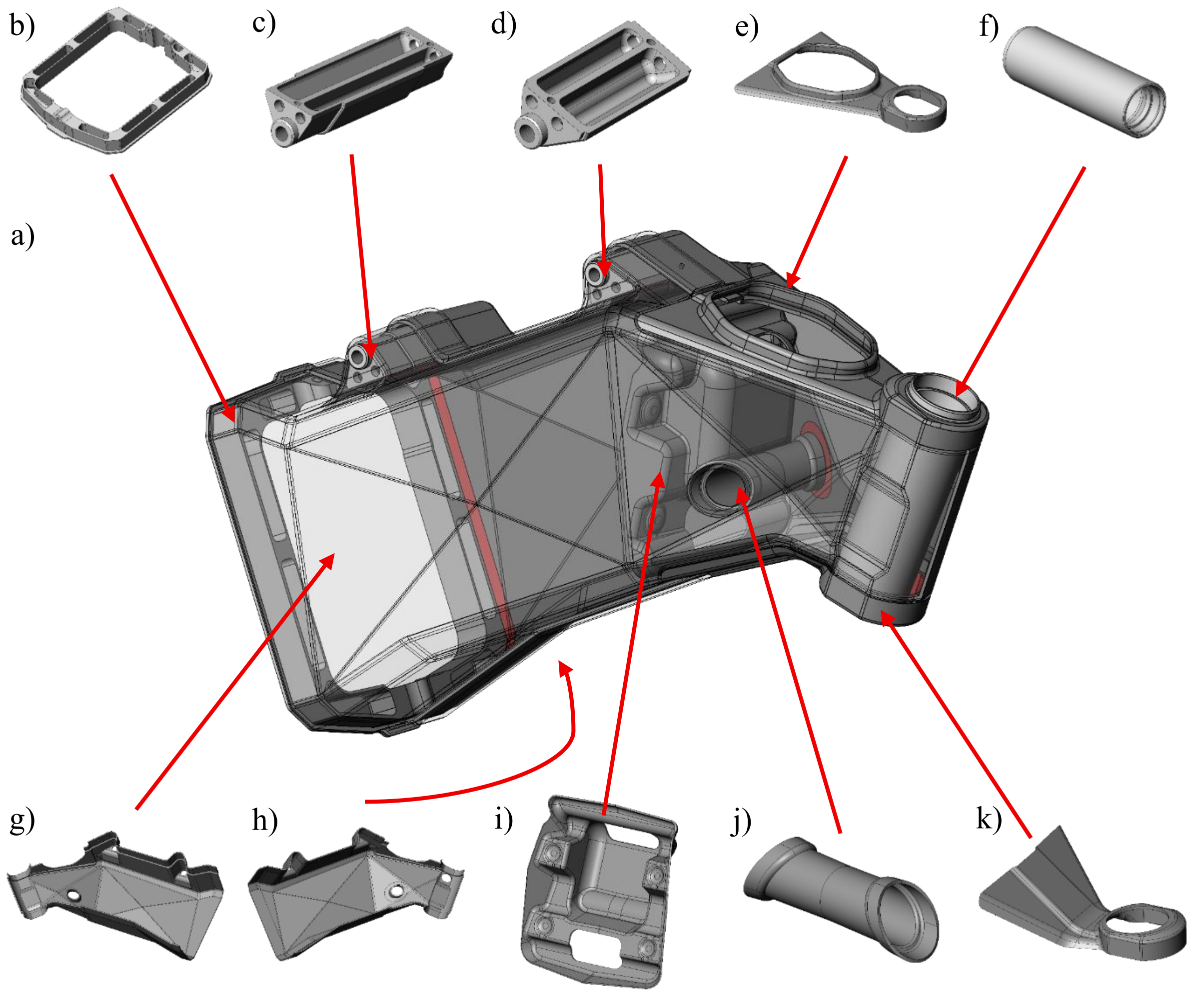

Fig. 7 Assembly of the baseline monocoque design a) monocoque assembly b) crankcase flange c) lower fuel tank insert d) upper fuel tank insert e) upper steering head f) steering head insert g) right half of monocoque h) left half of monocoque i) battery stop reinforcement j) cooling duct reinforcement k) lower steering head

2.3.3 Definition of load cases

Structural load cases

The target values for structural stiffness of the enduro motorcycle are summarised in Tab. 2. These should be regarded as minimum requirements, as the present analysis considers only the composite monocoque and not the complete frame. This simplification naturally reduces the absolute stiffness values compared to a full structure, although certain stiffening effects may arise from geometry. In addition, the reinforcing influence of the battery mounting system was not included in the simulations, which has a similar effect to comparing measurements performed with or without the engine. For these reasons, the stiffness targets are recommended reference values rather than absolute requirements.

Tab. 2 Structural simulation loading conditions

Stiffness	Enduro requirement	Loading	Expected deformation
Torsion	2500 Nm $°^{-1}$	1000 Nm	0,4 °
Longitudinal	4000 N mm^{-1}	1000 N	0,25 mm
Lateral	600 N mm^{-1}	1000 N	1,67 mm

Strength related load cases

Strength requirements focus on the safety of the structure under peak loads. To quantify these conditions, a simplified half-vehicle dynamic model of the motorcycle with two degrees of freedom was employed [28], with parameters corresponding to a motorcycle mass of 130 kg and a rider mass of 100 kg. This analysis identified three critical operating scenarios: braking, jump landing, and cornering. The resulting forces are summarised in Tab. 3, and their points of application are shown in Fig. 8. The load case landing appears twice in the table, as it reflects two distinct points of force application, each associated with a different load magnitude.

Tab. 3 Critical motorcycle load cases in operation

Load case	Point of application	F_X [N]	F_Y [N]	F_Z [N]
Braking	COG	2942	0	-2452
Landing	Suspension unit	-11126	0	-16620
Landing	Seat and footpegs	0	0	-1000
Cornering	Rear tire contact patch	0	-251	938

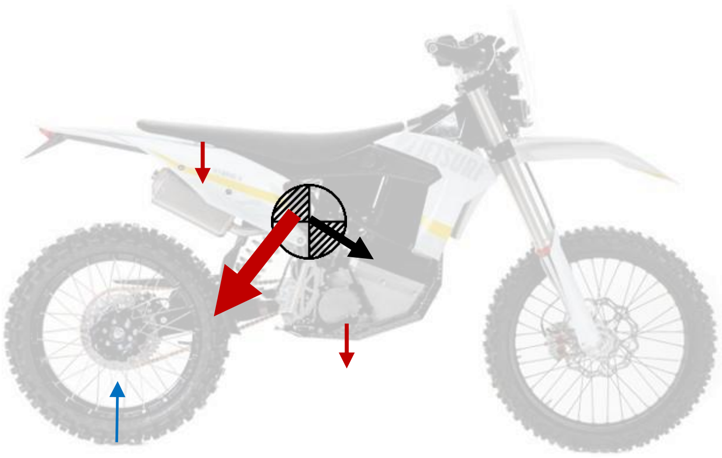

Fig. 8 Location and direction of loads during braking (black), landing from a jump (red), and cornering (blue); the circle in the centre indicates the position of the combined motorcycle–rider centre of gravity

3 MANUFACTURING TECHNOLOGY

The complete manufacturing process can be divided into several consecutive stages, starting with the fabrication of individual components and culminating in the final bonding of all subassemblies. The overall workflow is illustrated schematically in Fig. 9.

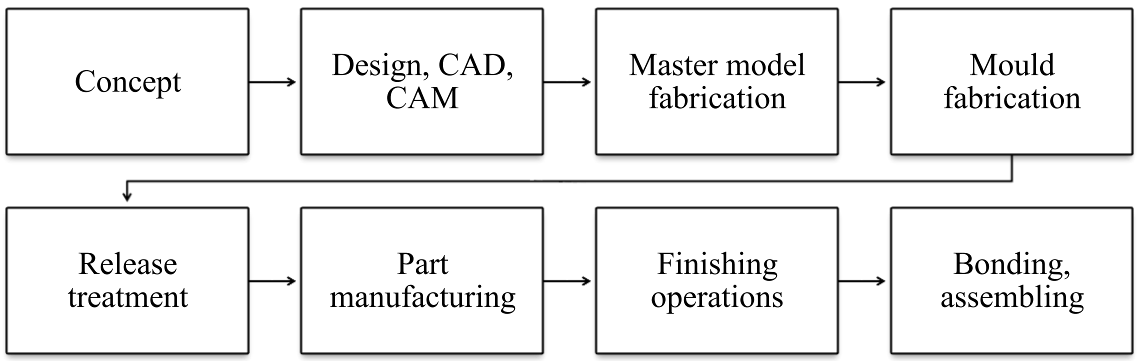

Fig. 9 Workflow of monocoque manufacturing process

3.1 MONOCOQUE PARTS

3.1.1 MONOCOQUE – RIGHT AND LEFT HALF

The fundamental structural components of the monocoque are the nearly symmetrical right and left halves (Fig. 10). They differ only in the presence of an external bonding flange on one half, which enables adhesive joining of the two shells into a complete structure. Already during the design stage, a minimum nominal wall thickness of 3 mm was specified. This value was used as the basis for the design of associated parts and for the definition of adhesive joints, which were dimensioned with a bond line thickness of 0.5 mm. Failure to maintain these tolerances could result in difficulties during assembly, including deformation of the bonded parts or an insufficient bond line.

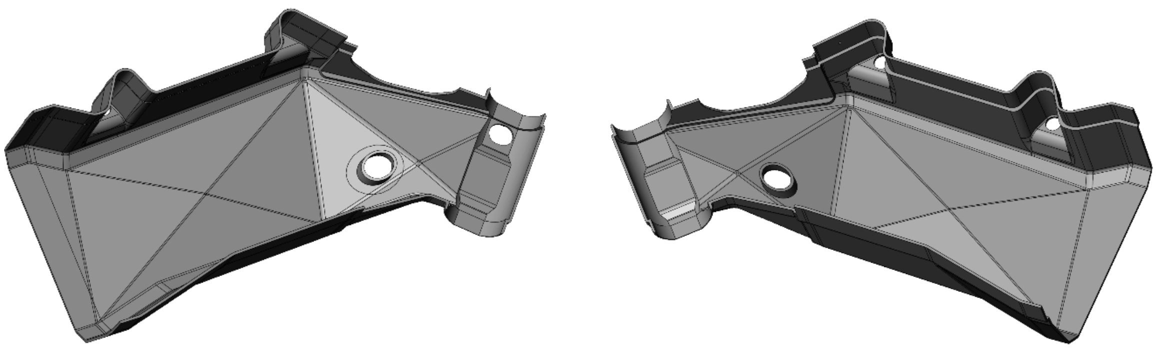

Fig. 10 Left and right half of monocoque (CAD)

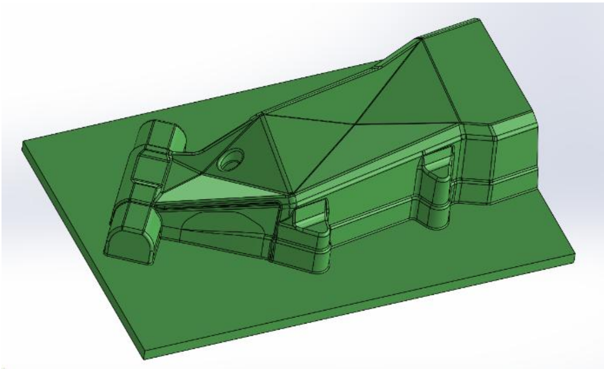


Fig. 11 Master model of left half of monocoque (CAD) and master model after machining


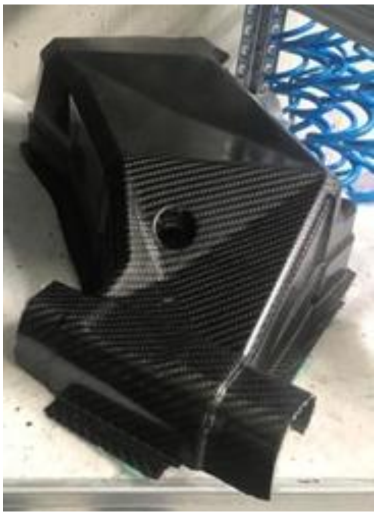

Fig. 12 Left: CFRP mould with a layer of woven fabric; Right: completed monocoque half prior to trimming.

3.1.2 Upper and lower steering head covers

The upper (Fig. 13) and lower steering head (Fig. 14) covers are structurally similar components, designed to serve as reinforcing lap joints in the steering head region. By overlapping the adhesive joint between the two monocoque halves, they simultaneously conceal the bond line and provide additional stiffness to one of the most geometrically constrained and heavily loaded areas of the frame (Fig. 15).

Their application, however, introduces several challenges. To achieve correct alignment and a visually coherent surface, very tight tolerances must be maintained during adhesive bonding. Even small deviations in nominal wall thickness can cause difficulties in assembly. Excessive bond line thickness may lead to misalignment of the covers, while insufficient thickness could result in incomplete joint formation.

Another demanding step is the trimming of the covers along their bevelled edges. Due to the complex geometry, trimming must be performed with high precision along the entire perimeter of the part. This is not only structurally important but also critical for ensuring that the joint line remains unobtrusive, thereby meeting both functional and aesthetic requirements.

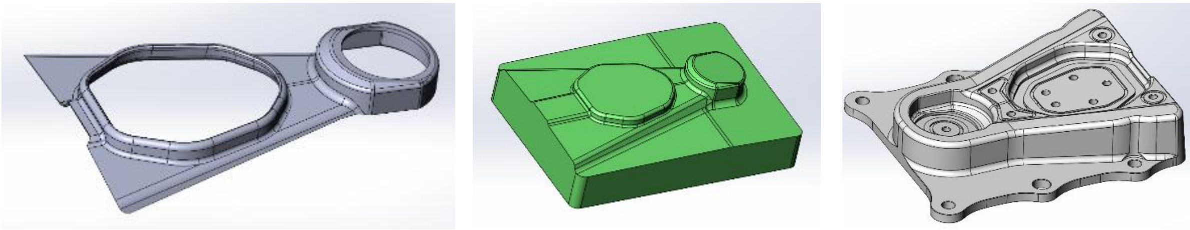

Fig. 13 Upper steering head cover part, master model and trimming fixture

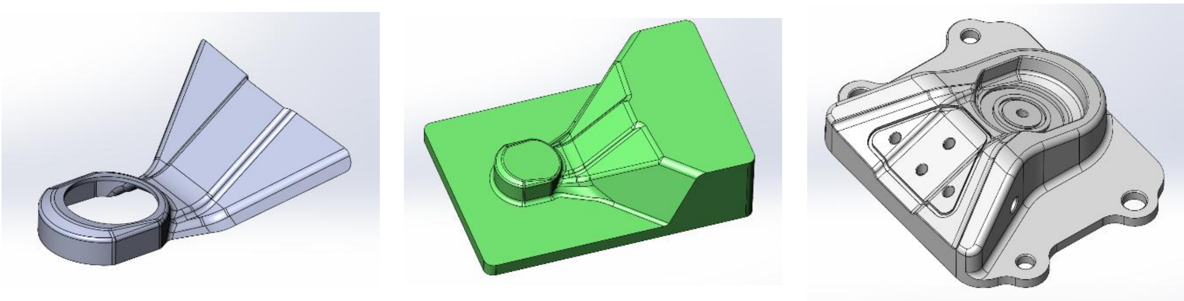

Fig. 14 Lower steering head cover part, master model and trimming fixture

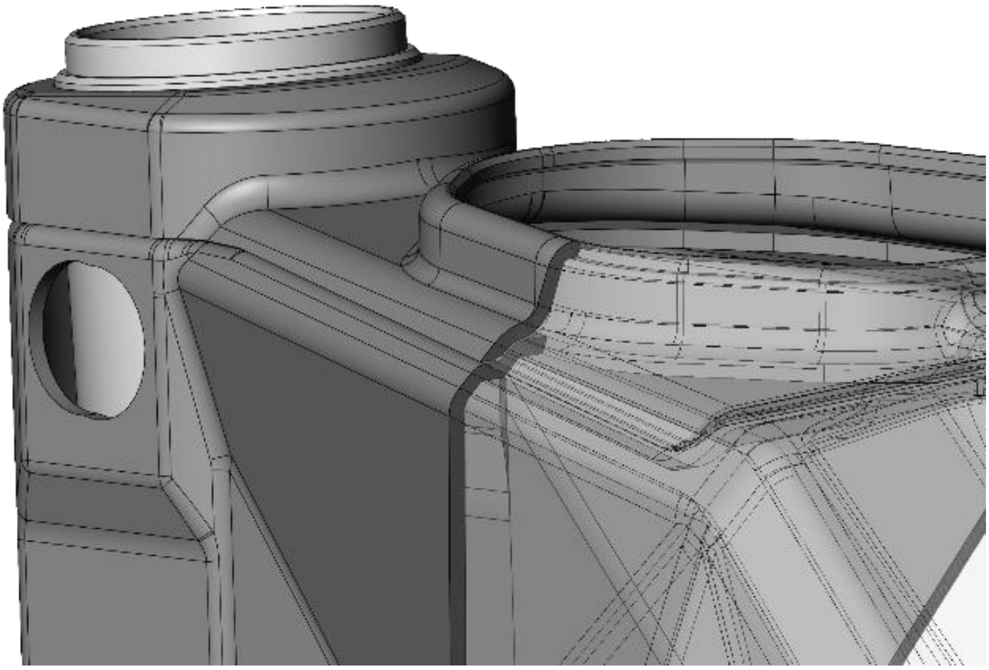

Fig. 15 Upper head cover monocoque overlap

3.1.3 Cooling duct and battery stop reinforcement

Two auxiliary components were integrated into the monocoque design, both of which fulfil multiple functions in addition to their structural role. The first component is a cooling duct, which mechanically protects the cooling hose routed through the monocoque. At the same time, it seals the opening to maintain the airtightness of the structure, enabling the monocoque to function as an airbox. Due to its position, it also provides a local stiffening effect. For the prototype series, the mould for this component was produced using 3D printing from polycarbonate (PC) material, which offers sufficient thermal resistance to withstand the pressure and temperature loads of autoclave curing. Under standard practice, the mould surface would require sanding; however, since the part is non-visual and the print layers were oriented perpendicular to the demoulding direction, only careful sanding of the edges was performed. The mould was nevertheless thoroughly release-treated, ensuring proper separation during demoulding. Although traces of the printed layers were visible, the part could be released without major issues.

The second auxiliary element is the battery stop, which also combines several functions. On one hand, it acts as a positioning feature that, with the use of rubber pads, prevents the battery from sliding deeper into the monocoque than intended. On the other hand, its geometry provides an additional reinforcing effect. This part was also produced as a non-visual component using the same 3D printing method. Despite its considerably complex geometry, the mould surface was covered with a PTFE film, which eliminated the need for further finishing and allowed direct lay-up on the surface (Fig. 18).

The main reasons for selecting 3D printing were the speed of production and the possibility of manufacturing prototype moulds without extensive post-processing. These benefits were particularly valuable for the early development stages, where rapid verification of design concepts was prioritised over long-term mould durability.

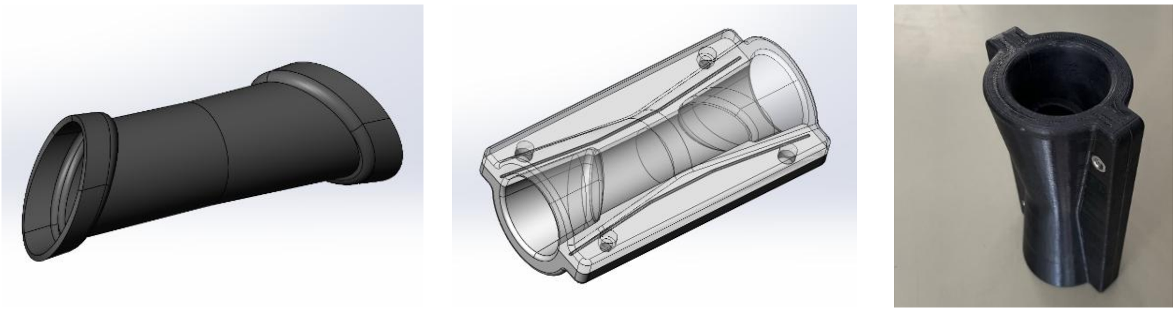

Fig. 16 Cooling duct, cooling duct mould and 3D printed mould

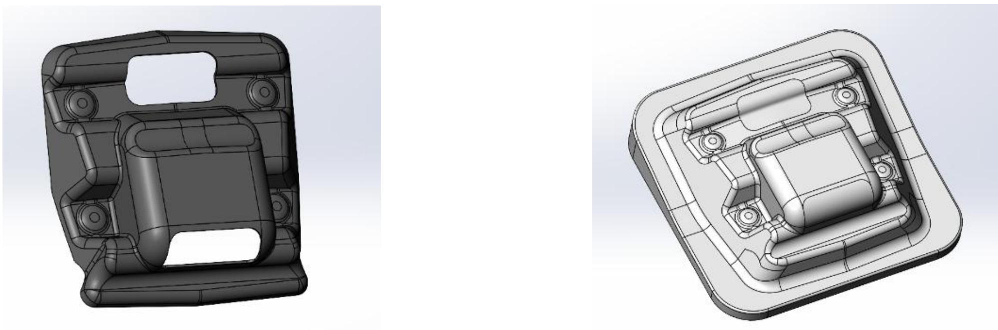

Fig. 17 On the left: battery stop reinforcement part; on the right: CAD model of 3D printed mould

Fig. 18 3D printed mould with PTFE film

3.2 BONDING OF THE STRUCTURAL ASSEMBLY

The final stage of manufacturing involves the bonding of all composite and aluminium components into a complete structural monocoque. Adhesive bonding was selected as the joining method due to its ability to distribute stresses uniformly, reduce stress concentrations compared to mechanical fastening, and maintain low structural weight.

For the prototype series, the epoxy adhesive 3M DP 490 was employed. This adhesive was chosen for its long pot life, which provides sufficient working time for the accurate positioning of parts, and for its tolerance to variations in bond-line thickness. Bonded joints were designed with a nominal gap of 0.5 mm, which was verified using control gauges. An additional advantage of this adhesive is that its shear strength does not decrease significantly with increasing bond-line thickness, making it particularly suitable for prototype assemblies where slight dimensional variations may occur.

Prior to bonding, the surfaces were prepared according to standard industrial practice. Areas intended for adhesive joining were either covered with peel ply during the lay-up process or subsequently abraded and chemically cleaned to ensure sufficient surface energy. Peel ply surfaces were preferred wherever possible, as they provided a roughened surface without the risk of contamination associated with mechanical abrasion.

The bonding process proved to be one of the most challenging stages of the monocoque manufacturing workflow. Among the main difficulties were the non-uniform laminate thickness and the suboptimal overlap design, which occasionally resulted in visible black seams caused by adhesive residues. These seams, although later concealed under the clear paint layer, illustrate the sensitivity of the process to dimensional tolerances.

It should be emphasised that the work was conducted under prototype conditions, primarily aimed at verifying the feasibility of the concept while conserving resources. For this reason, a simplified bonding fixture was employed, with the understanding that in future iterations it would be replaced by a more robust aluminium fixture with integrated clamps.

3.2.1 BONDING FIXTURE

The provisional fixture is illustrated in Fig. 19. It was manufactured using 3D FDM printing, where printed supports for the individual parts were mounted onto a 20 mm MDF raster plate. Although MDF is prone to warping under humidity and 3D-printed parts are not dimensionally perfect with inadequate stiffness, this solution represented an acceptable compromise at the prototype stage.

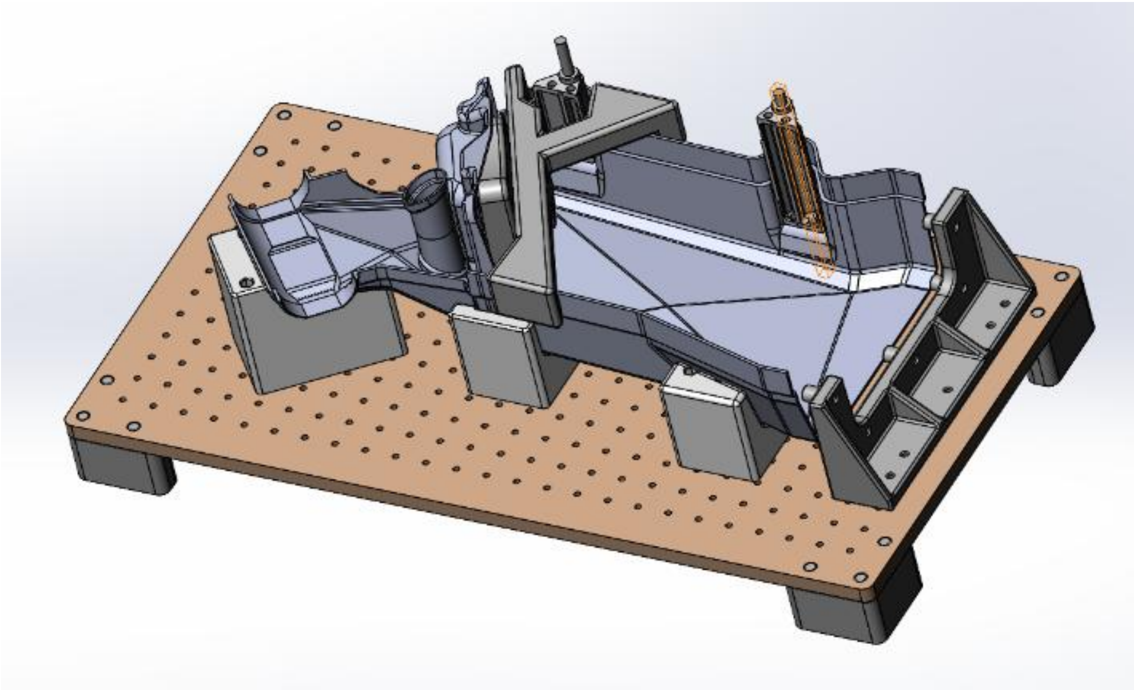

Fig. 19 Bonding fixture

3.2.2 BONDING SEQUENCE – PHASE I

In the first phase, the right half of the monocoque was positioned in the fixture. The part remained loosely supported until the adhesive was applied. Inserts for the fuel tank mounts were bonded by injecting adhesive into the designated cavities. Each insert contained steel pins protruding from its lower side, which engaged with corresponding holes in the fixture, thereby ensuring correct positioning. Adhesive was not spread up to the very edge of the bonding flange but rather applied approximately 3 cm below it. Correct alignment was further maintained by an additional printed guide placed from the upper side, which engaged with the flange and defined the insert position.

At the rear of the monocoque, adhesive was applied to the area intended for the aluminium flange connecting the monocoque to the engine crankcase. The flange was inserted with maximum care to minimise adhesive removal during sliding contact. The geometry of the demoulding angle reduced this effect, and final positioning was again ensured by 3D printed fixture elements.

Subsequently, adhesive was applied to the location of the hose pass-through. Here, correct alignment was achieved through the interaction with the battery stop, which was pre-assembled with the fixture. The battery stop was bonded by applying adhesive to one half of the monocoque, pressing the component into place, and clamping it using the fixture, which located the flange precisely.

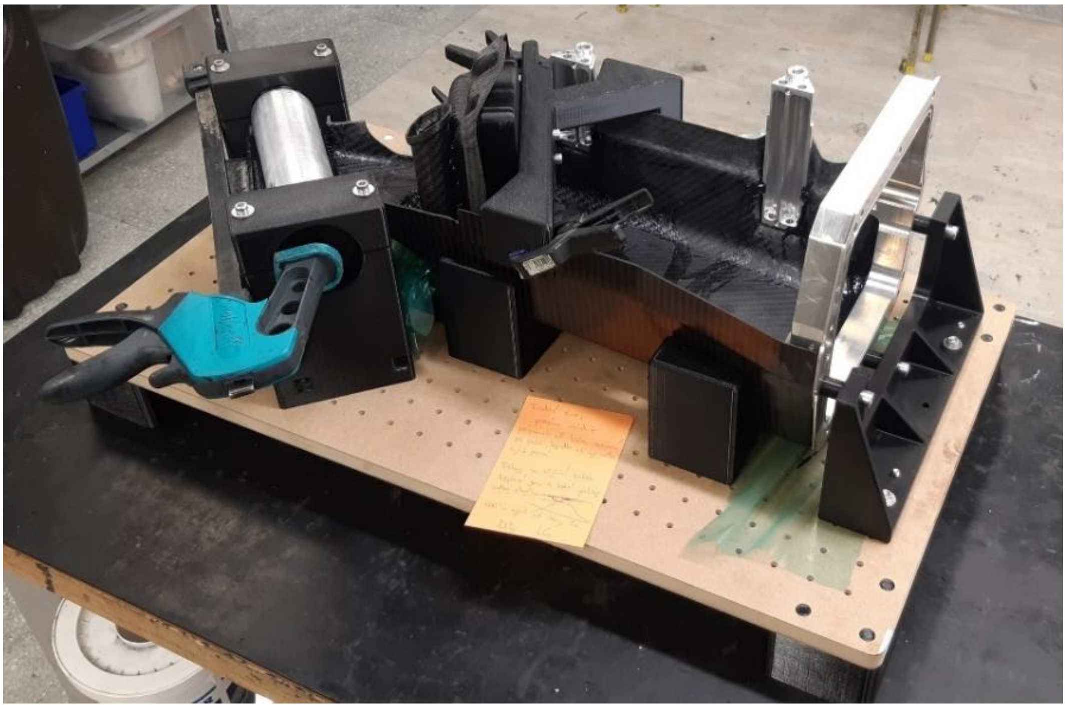

Fig. 20 Bonding fixture after phase I.

For reasons of confidentiality, the bonding and construction details of the steering head insert are not presented in this dissertation, as they form part of a protected solution.

3.2.3 BONDING SEQUENCE – PHASE II

After approximately six hours, once the adhesive reached handling strength, the second phase of bonding could begin. At this stage, the left half of the monocoque remained positioned in the fixture with all inserts and auxiliary components already bonded. Before placing the second half, adhesive was applied not only to the bonding flange of the right half—so that any excess would be displaced towards the inside of the joint rather than outward to the visible edge—but also to all remaining mating surfaces of the inserts and auxiliary components. This ensured that all contact areas were sufficiently covered with adhesive prior to closing the assembly.

The right half was then aligned and pressed against the left half. Due to the prototype nature of the fixture, slight variations in laminate thickness occasionally led to visible seams where adhesive was squeezed out. Although these seams later became visually unobtrusive beneath the clear paint layer, they highlight the sensitivity of the bonding process to manufacturing tolerances.

Following the assembly of the halves, adhesive fillets were formed in the interior corners to enhance joint strength and to prevent stress concentrations. In this prototype case, the assembly was loaded with external weight to maintain uniform contact along the joint during curing. The adhesive was allowed to cure at room temperature until full polymerisation was achieved.

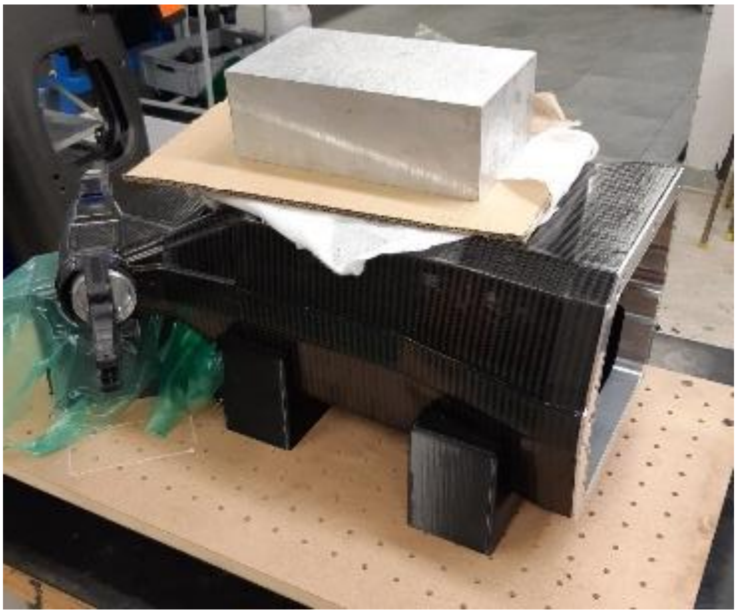

Fig. 21 Bonding fixture after phase II.

3.2.4 BONDING SEQUENCE – PHASE III

After completion of the second bonding phase, the remaining components to be attached were the upper and lower steering head covers. In this step, adhesive was applied over the entire mating surface, and the covers were fixed to the monocoque using mechanical clamps to maintain contact during curing.

This solution, however, proved challenging. Due to the laminate thickness variations and the bevelled geometry of the steering head, it was difficult to achieve perfectly uniform fixation of the two covers relative to the monocoque. Careful removal of excess adhesive squeeze-out was therefore required to prevent visual or structural defects.

Following bonding, the assembly underwent post-processing. The entire monocoque surface was sanded to achieve a uniform finish, enabling subsequent application of the protective and aesthetic paint layer. Fig. 22 shows the completed monocoque integrated into the motorcycle frame.

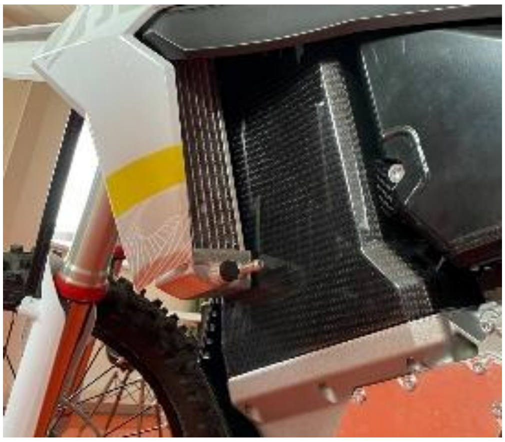

Fig. 22 Completed monocoque integrated into motorcycle

4 MATERIAL PROPERTIES AND DATA VALIDATION

To ensure that the conducted simulations and optimisation procedures correlate with reality, dedicated material specimens were manufactured and tested. The aim was to determine the fundamental mechanical properties of the biaxial reinforcements and woven fabrics used in this study. These experimentally obtained values served as the basis for defining the material models applied in the numerical analyses. The measured values are specified in doctoral thesis.

4.1 TECHNOLOGICAL SPECIMEN

To validate that the numerical simulations converge towards reality, a technological specimen was employed which was both structurally and technologically very similar to the investigated frame. The advantage of this approach lies in the fact that measurements of its structural properties had already been carried out [29]. Therefore, only simplified simulations needed to be performed—focusing not on obtaining absolute values, but rather on enabling comparative assessment between different design variants—and subsequently verified against the experimental data. Since the overall objective of this work is structural optimisation, even in the case where simulated results do not converge within a narrow tolerance to the measured values, they can still be considered sufficiently consistent to allow a meaningful comparison among the investigated design alternatives.

4.1.1 CONSTRUCTION OF THE TECHNOLOGICAL SPECIMEN

A technological specimen was employed that featured a construction, layup, and manufacturing technology closely resembling those of the proposed frame design. The selected specimen was an adhesively bonded composite swingarm [29], illustrated in Fig. 23.

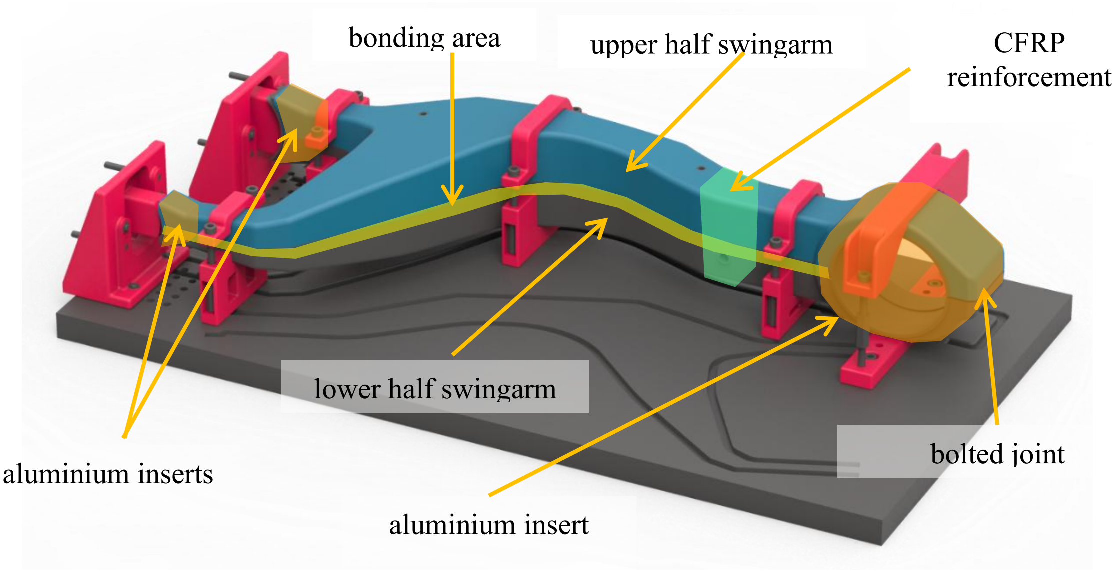

Fig. 23 Construction of the technological specimen

4.1.2 VALIDATION RESULTS

The stiffness distributions obtained from simulations and experimental measurements are presented in Fig. 24 and Fig. 25. Both torsional and longitudinal stiffness exhibit a linear dependence on load in the higher ranges. At lower load levels, however, the measured deformations were affected by fixture play and experimental inaccuracies, and therefore the results corresponding to the lowest applied forces were not considered. Overall, the results demonstrate a high degree of convergence between simulation and experimental data. It can thus be concluded that the material model is correctly defined in terms of elastic orthotropic coefficients, and that subsequent simulations provide relevant and reliable results.

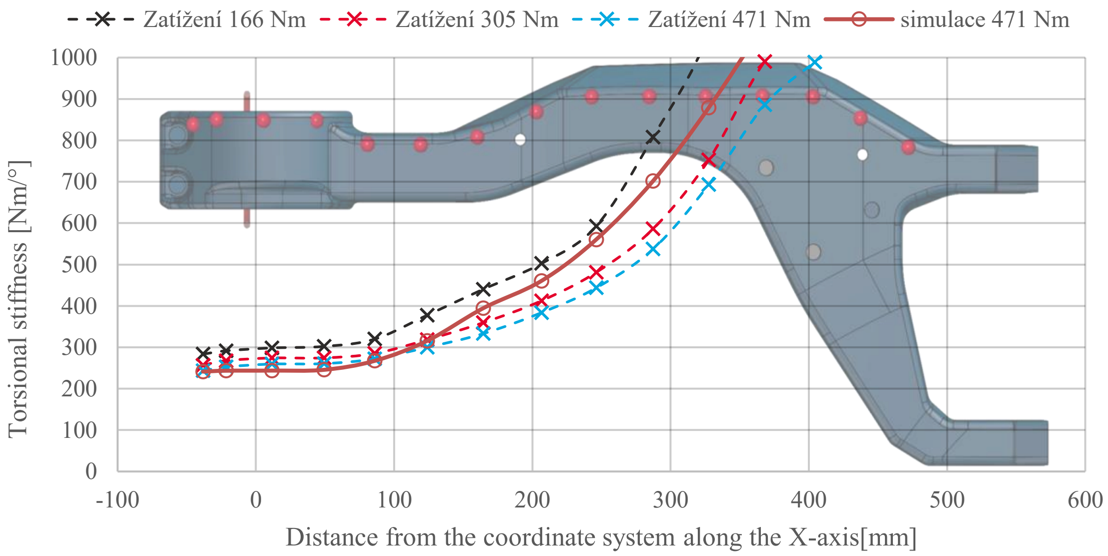

Fig. 24 Comparison of simulated and measured torsional stiffness

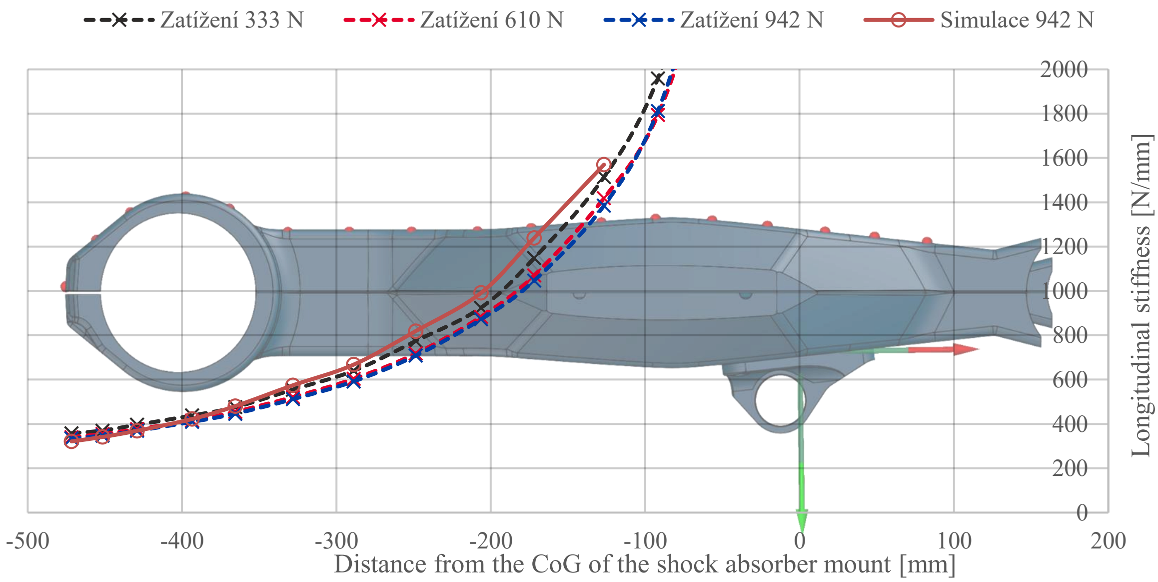

Fig. 25 Comparison of simulated and measured longitudinal stiffness

Tab. 4 Comparison of global stiffness values

Load type	Applied load	Simulation	Measurement	Difference
Torsion	471 Nm	241 Nm $^{\circ -1}$	243 Nm $^{\circ -1}$	0,8 %
Longitudinal	942 N	322 N mm^{-1}	322 N mm^{-1}	3,7 %

5 TOPOLOGY OPTIMISATION

5.1 PRIMARY DESIGN ITERATION

5.1.1 DESIGN SPACE

Topology optimisation of a carbon fibre motorcycle monocoque requires precisely defined boundary conditions. These include not only the specification of loads and supports, but also the geometric constraints arising from the packaging of other components, as detailed in chapter 2.3.1. Such constraints determine the design space for optimisation and define the extent to which the structure can be modified in shape or function without compromising operability, ergonomics, or subsystem integration.

Based on these requirements, an initial geometric model was developed to establish the fundamental design space for optimisation. A sectional view of the resulting design space is presented in Fig. 26.

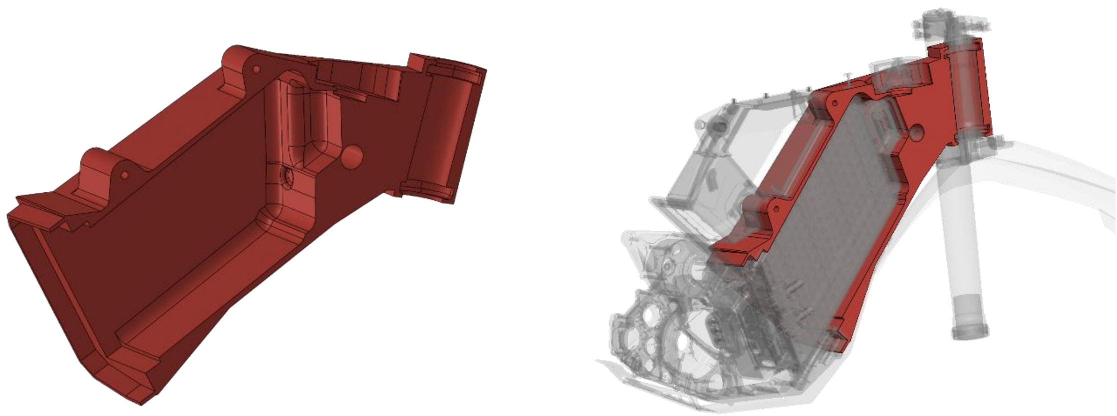

Fig. 26 Initial iteration of the topology optimisation, left: section through the design space, right: section through the design space in the context of the motorcycle assembly.

5.1.2 OPTIMISATION SETUP

The optimisation setup in this case was relatively complex, as the material properties defined for the optimisation model differ from those that will be applied in the final design. After interpreting the optimisation results, the isotropic material initially used will be replaced by an anisotropic composite laminate, and further modifications are introduced to reflect manufacturing constraints typical for thin-walled shell structures.

To obtain results as relevant as possible, aluminium was selected as the baseline optimisation material. Its Young's modulus of 71 GPa is close to the calculated effective stiffness of the CFRP laminate in both the longitudinal (E_0) and transverse (E_{90}) directions. For the purpose of the optimisation, the modulus was reduced to approximately match E_0, which—although neglecting anisotropy—provides a reasonable approximation of the laminate stiffness through the thickness.

For the optimisation domain, the entire volume of the part was included. Only regions with prescribed constraints or loads were excluded from optimisation, ensuring that structural connections and boundary conditions remained intact.

Tab. 5 Comparison of reference stiffness values

Material	Young's modulus of elasticity		
Steel	210 GPa		
Aluminium	71 GPa		
CFRP K (0°/45°/0°/45°/0°)	E_0	E_{45}	E_{90}
	51 GPa	43 GPa	51 GPa

The optimisation objectives are summarised in Tab. 6. The primary objective was to reduce the material volume by 40 %, while simultaneously minimising stress under braking, jump, and cornering load cases, and minimising compliance under torsional, longitudinal, and lateral load cases.

Tab. 6 Optimisation objectives

Response type	Goal	Load case	Weight	Response constraint
Volume	Minimize	-	1	40 %
Stress	Minimize	Braking	1	-
Stress	Minimize	Jump	1	-
Stress	Minimize	Cornering	1	-
Compliance	Minimize	Torsion	1	-
Compliance	Minimize	Longitudinal	1	-
Compliance	Minimize	Lateral	1	-

All objectives were assigned equal weighting. Apart from the volume reduction target, the remaining objectives did not have discrete numerical constraints. As a result, the algorithm aimed to find a compromise material distribution that globally minimised compliance and stress concentrations, without converging to specific target values in individual load cases.

The Mixable Density Method was used for the multi-load topology optimisation. With multiple load cases and a single volume constraint, the solver does not attempt to satisfy explicit limits for deformation or stress. Instead, it minimises the strain energy (compliance) by combining contributions from the different load cases. In practice, this means that some load cases drive the structure towards higher stiffness, while others suppress stress concentrations. The outcome is a material distribution that, for the prescribed 40 % volume reduction, delivers the best compromise of global stiffness and uniform stress distribution Fig. 27.

Finally, an additional symmetry constraint was imposed. Because some of the load cases are not perfectly symmetric with respect to the motorcycle's longitudinal plane (e.g. forces acting on the offset suspension unit, or torsional loading applied in a single direction), a symmetry condition about the Y-plane was enforced to ensure a geometrically balanced design.

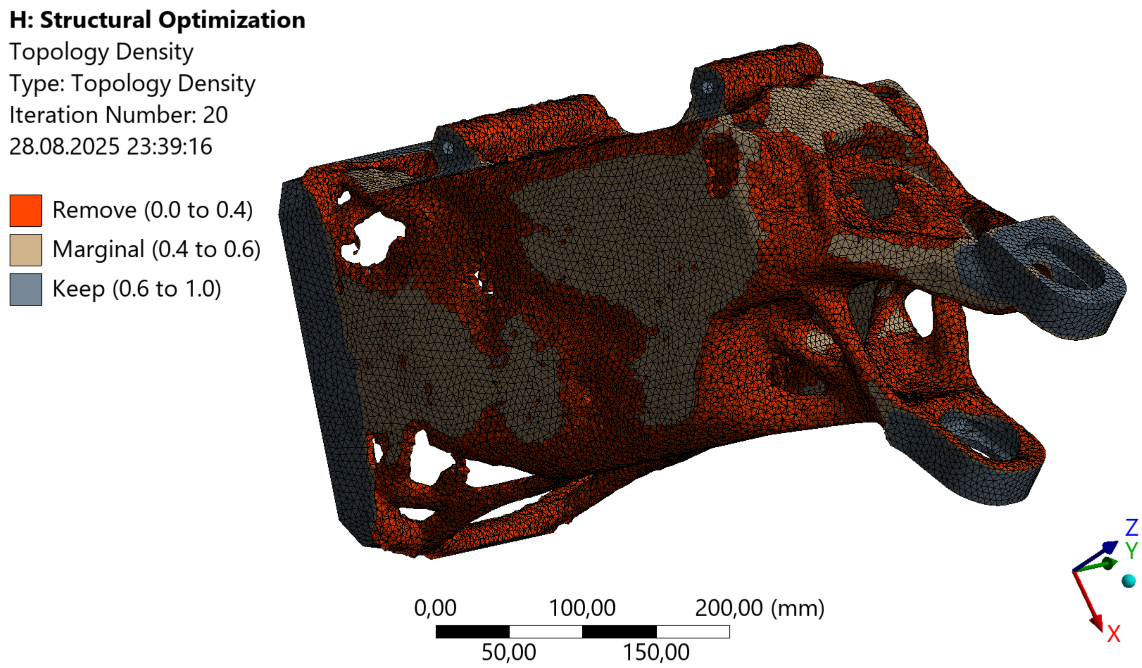

Fig. 27 Result of topology optimisation

5.1.3 Results and interpretation

The initial geometry of the monocoque frame had a mass of 11.9 kg. After topology optimisation, this value was reduced to 5.7 kg, representing a weight reduction of more than 50 %.

The key task following the topology run was to correctly interpret the generated geometry and to modify it into a feasible design. At this stage, it was necessary to already take into account the manufacturing technology and to propose modifications or alternative approaches where the original output could not be realised directly.

Fig. 28 illustrates the overlay of the optimised material distribution with the input geometry. In the rear section of the monocoque, only minor changes were possible due to the limited design space constrained by the battery system. In this area, the modifications mainly corresponded to shape optimisation of the gross geometry – removal of sharp corners, smoothing of surfaces, and elimination of small radii – motivated both by mechanical performance and by manufacturability.

More significant changes were observed in the steering head region, where the optimisation suggested a notable slimming of the structure and removal of redundant volumes. Based on the load distribution obtained earlier, an internal stiffening structure was introduced into this area. This additional geometry provided the required stiffness without unnecessarily increasing mass. The details of this step are discussed in the following chapter.

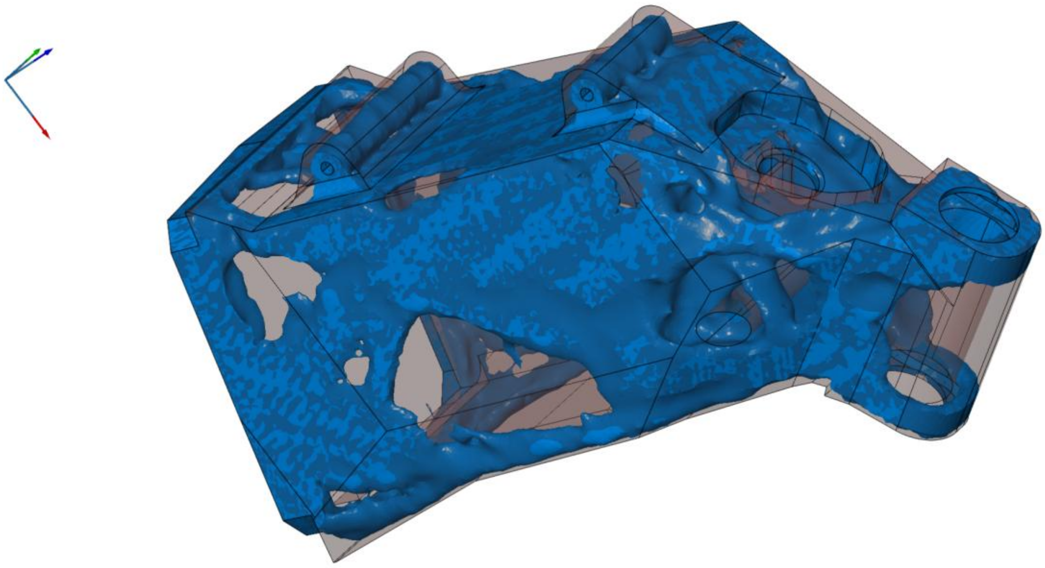

Fig. 28 Overlay of the optimised material distribution with original geometry

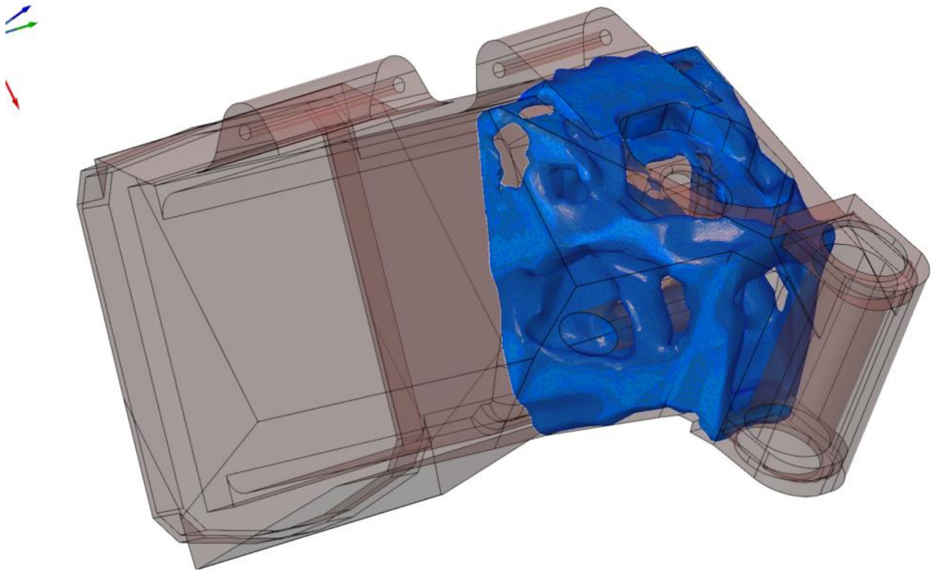

Fig. 29 Optimised material distribution in the neck area

6 DESIGN AND MANUFACTURING OPTIMISATION

Based on the results of the topology optimisation, together with the experience gained from the prototyping and manufacturing of the baseline composite monocoque, a series of design modifications were proposed. The primary goal of these changes was to simplify and streamline production, reduce the number of parts and associated tooling, and eliminate known technological issues encountered during prototype fabrication. At the same time, the modifications aimed to increase the mechanical performance of the frame while keeping the overall lay-up scheme and production costs at a comparable level.

The overall concept of the bonded assembly remains unchanged. However, several geometrical and structural improvements were introduced to enhance the manufacturability of the monocoque, to facilitate handling during the lay-up and bonding processes, and to ensure more reliable structural performance in operation.

6.1 LIMITATIONS OF THE BASELINE DESIGN

The initial prototype design revealed a number of limitations that affected both manufacturing efficiency and the quality of the final structure:

- Nominal thickness constraints. In several critical regions, the laminate thickness could not be adapted to the structural requirements. Moreover, the application of sandwich structures with lightweight cores was not feasible due to the complex geometry.

- Fuel tank mount inserts. Aluminium holders for the fuel tank were embedded into the composite shell through small, difficult-to-machine pockets. These features not only required extensive CNC machining but also demanded multiple orientation changes of the lay-up. The limited bonding area, combined with overlaps of prepreg plies, frequently resulted in local deviations in laminate thickness, which complicated the positioning of inserts and led to uneven adhesive bond lines.

- Bonding flange design. The flange was originally oriented outward, which indeed allowed the use of a one-piece mould but produced a visible joint line on the otherwise smooth outer surface of the monocoque. This required subsequent filling and finishing to conceal the cut carbon fibres. The flange geometry also increased the risk of adhesive being wiped off during assembly, reducing bond reliability.

- Complex external geometry. The outer surface of the shell contained numerous small radii, sharp corners, and deep recesses, which not only hindered the placement of larger prepreg plies but also made the fabrication of the master model and mould significantly more labour-intensive.

- Sharp radii and edges. Small radii increased the risk of defects such as bridging, voids, wrinkling of fibres, and poor consolidation during vacuum bagging and curing. These features also raised the probability of local stress concentrations and delamination under load.

- Bonding accuracy. During the bonding of the two halves, the assembly lacked reliable physical stops to define the final position of the parts. Variations in laminate thickness combined with rounded edges at the flanges made precise alignment difficult, often leading to uncontrolled bond-line thickness.

Overall, the baseline prototype monocoque highlighted the necessity to simplify the geometry, redesign critical inserts and bonding flanges, and improve tolerance management. These lessons, together with the guidelines from the optimisation study, formed the basis for the new design modifications presented in the following sections.

6.2 OPTIMISED DESIGN

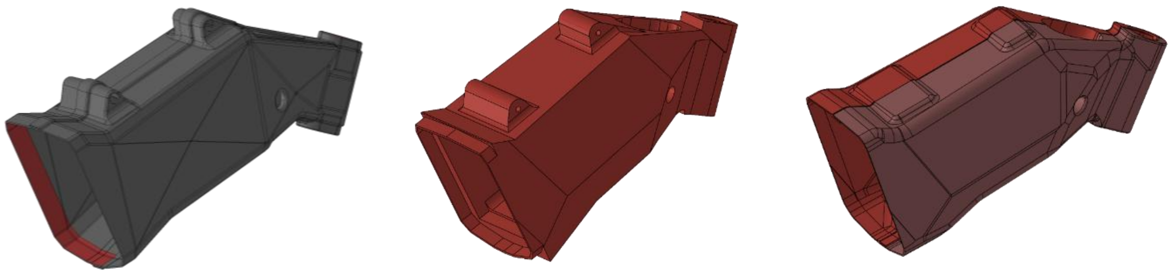

Fig. 30 Left: baseline design; middle: topology optimisation input; right: optimised design

6.2.1 INTRODUCTION OF AN INTERNAL RIB

The most significant design change introduced on the basis of topology optimisation was the addition of an internal rib structure in the steering head region (Fig. 31). This reinforcement follows the load paths identified in Chapter 5 and locally increases stiffness in one of the structurally weakest parts of the frame. At the same time, the rib also functions as a stop element for battery positioning during installation, thus combining structural and functional roles.

In the selected configuration, the rib is manufactured separately and subsequently bonded into the cured monocoque shell. This approach offers flexibility in fabrication and quality control of the rib, while allowing the main monocoque halves to be produced without additional complexity in the mould. Although it requires an additional bonding operation and introduces tolerances in the adhesive bond line, these disadvantages are outweighed by the advantages in manufacturability and modularity.

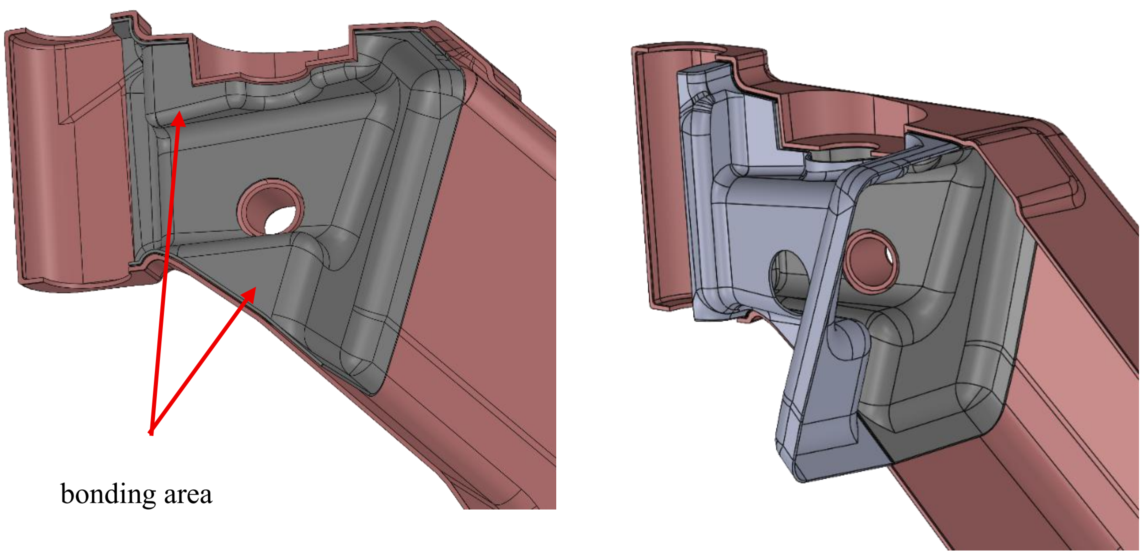

Fig. 31 Steering head region reinforcement

A further benefit of this arrangement is that the space between the two ribs forms a continuous thin bond line, which not only provides a secure adhesive joint but also contributes to the reinforcement of the steering head region by coupling both rib elements across the joint.

6.2.2 REDESIGN OF FUEL TANK MOUNTS

The baseline design included aluminium holders for the fuel tank embedded into small pockets within the laminate. These pockets were difficult to manufacture and created local thickness variations, which caused complications during adhesive bonding. In the optimised concept, these features were eliminated (see Fig. 30). Instead, a simplified insert is bonded into an internal cavity of the shell, while the external fuel tank bracket will be mounted from the outside and screwed directly into the insert. The insert itself is designed as a turned part with an integrated thread and shoulder, which is bonded into the composite wall. This solution reduces manufacturing complexity, improves bonding reliability, and lowers costs by allowing the external bracket to be produced by simple bending, welding, or straightforward machining.

6.2.3 MODIFICATION OF BONDING FLANGES

In the baseline design, the bonding flange was oriented outward, which created visible joints on the external surface and increased the risk of adhesive being wiped off during assembly. In the optimised concept, the two halves are joined using an internal lap joint, which conceals the bond line and provides a much cleaner appearance.

The flange geometry was further modified by introducing a small chamfer (bevel) at the flange edge. This reduces the likelihood of adhesive being scraped away when the halves are pressed together, thereby improving the reliability and uniformity of the joint. As a result, the overall consistency and robustness of the bonding process are significantly enhanced.

This modification also influences the tooling concept. Since the lap joint is recessed inward, the mould can no longer be manufactured as a one-piece tool. Instead, an opposing tool surface (counterpart) must be incorporated along the parting line to create the necessary flange offset towards the inside of the monocoque.

6.2.4 OVERALL SMOOTHING OF GEOMETRY

The optimised geometry from Chapter 5 was taken as the baseline, but it was subsequently simplified to meet manufacturing constraints. Sharp corners, small radii, and unnecessary recesses were eliminated, resulting in smoother surfaces that facilitate lay-up and reduce the risk of typical composite defects such as bridging, wrinkling, or voids. This also enables the use of larger prepreg plies, decreases the number of overlaps, and improves laminate quality and process repeatability.

6.2.5 REDUCTION OF PART COUNT

An additional step towards simplifying the design was the reduction in the total number of composite parts forming the bonded assembly. This modification directly results in fewer moulds, fewer assembly fixtures, and a reduced number of bonding operations. Consequently, manufacturing efficiency is increased, while the probability of dimensional inaccuracies during assembly is reduced. In the optimised configuration, the monocoque consists of only four composite components instead of six—the two main halves and the newly added internal ribs.

6.2.6 MULTI-PIECE MOULD

The last modification concerned the integration of the intake filter pocket directly into the monocoque structure. In the baseline prototype, this pocket was realised as a separate plastic insert placed into an opening in the composite shell. In the optimised design, however, the pocket is incorporated directly into one half of the monocoque, which simplifies assembly but simultaneously requires the use of a multi-piece mould.

The necessity of a multi-piece tool is further reinforced by the inward offset of the bonding flange, which prevents demoulding of the part using a single-piece mould. In this case, the problem is solved by a simple shaped insert mounted into the cavity of the monocoque half. The insert is attached to the mould wall by screws. Since the part is not a visible component, minor dimensional inaccuracies are acceptable, and the insert does not require precise dowel pin positioning. After curing, the screws are removed and the insert can be released together with the part, ensuring straightforward demoulding.

7 NUMERICAL ANALYSIS OF MONOCOQUE STRUCTURES

Numerical simulations were carried out for both the baseline version of the monocoque and an optimised variant that incorporates the results of topology optimisation and structural simplifications.

7.1.1 TORSION LOADING

For the torsional load case, a torque moment was applied to the aluminium flange connecting the engine crankcase to the frame. The moment acts along an axis passing through the centroid of the loaded surface, perpendicular to the steering axis, and lying in the plane of symmetry of the motorcycle. On the inner surface of the aluminium insert of the steering head, a fixed support was defined, constraining all degrees of freedom. The resulting torsional angle of twist was determined based on the lever arm between the torsional axis and the point at which displacement due to deformation was measured. From these values, the torsional stiffness was calculated. Results are summarized in Tab. 7.

Tab. 7 Composite monocoque torsional stiffness results

	Baseline design	Optimised design	Percentual difference
Applied load	1 000 Nm	1 000 Nm	
Displacement of point	0.89 mm	0.39 mm	- 56 %
Lever arm length	121 mm	121 mm	
Angle of twist	0.421°	0.185°	+ 56 %
Torsional stiffness	2 376 Nm $^{\circ-1}$	5 405 Nm $^{\circ-1}$	+ 128 %
Mass	2.43 kg	2.38 kg	- 2 %

7.1.2 LONGITUDINAL LOADING

For the longitudinal load case, a force was applied at the intersection of the steering-head axis and the front-wheel axle. The force acted perpendicularly to the steering-head axis and was transferred to the inner surface of the aluminium insert of the fork mounting, thereby inducing a bending moment in the frame. On the contact surface of the aluminium insert connecting the frame to the crankcase, a fixed support was defined, constraining all degrees of freedom. The resulting longitudinal displacement used for stiffness evaluation was obtained from the measured shift of a reference point on the lower edge of the steering-head insert. The calculation was based on the trigonometric relation of the tangent function between the measured displacement and the corresponding lever arm to the load application point. From these values, the longitudinal stiffness was determined. The results are summarised in Tab. 8.

Tab. 8 Composite monocoque longitudinal stiffness results

	Baseline design	Optimised design	Percentual difference
Applied load	1 000 N	1 000 N	
Average displacement of reference point	0.25 mm	0.15 mm	- 40 %
Lever arm from rotational axis	92 mm	92 mm	

Lever arm to load application point	913 mm	913 mm	
Displacement at load application point	2.48 mm	1.49 mm	- 40 %
Longitudinal stiffness	403 N mm^{-1}	671 N mm^{-1}	+ 67 %
Mass	2.43 kg	2.38 kg	- 2 %

7.1.3 LATERAL LOADING

For the lateral load case, a force was applied to the surface of the aluminium flange connecting the engine crankcase to the frame. The force acted in the lateral direction and was applied with an offset along the Z-axis in order to minimise the unintended torsional loading. A fixed support was defined on the inner surface of the aluminium insert of the steering head, constraining all degrees of freedom. The resulting lateral displacement was obtained from the measured shift of a designated reference point. From these values, the lateral stiffness was determined. The results are summarised in Tab. 9.

Tab. 9 Composite monocoque lateral stiffness results

	Baseline design	Optimised design	Percentual difference
Applied load	1000 N	1000 N	
Average reference point displacement	2.08 mm	0.87 mm	- 58 %
Lateral stiffness	480 N mm^{-1}	1150 N mm^{-1}	+ 140 %
Mass	2.43 kg	2.38 kg	- 2 %

7.2 STRENGTH PARAMETERS

For the evaluation of composite failure, three widely recognised criteria were applied: maximum strain, maximum stress, and Tsai–Wu. These criteria were selected because they together provide a comprehensive description of laminate behaviour. The maximum strain and maximum stress criteria enable a straightforward assessment of whether individual ply stresses or strains exceed the corresponding material limits, while the Tsai–Wu criterion offers a more general failure envelope that accounts for multi-axial stress states and interaction effects between different stress components.

The target was to maintain a safety factor of 3 for all load cases, which corresponds to an inverse reserve factor (IRF) of 0.33. Areas where the IRF falls below this threshold indicate insufficient safety and require further reinforcement or redesign. Since local maxima occurs due to mesh imperfections or discretisation artefacts, the comparison between design variants is based primarily on the average IRF values across the component. This approach filters out isolated outliers and provides a clearer and more representative basis for comparison.

7.2.1 BRAKING

The applied boundary conditions are identical to those used for the topology optimisation. From a safety perspective, the baseline geometry exhibits critical regions where the inverse reserve factor (IRF) exceeds 0.33 across all applied failure criteria. These regions act as local stress concentrators, primarily due to the presence of small and sharp radii. In the optimised geometry, similar exceedances can also be observed, but they occur to a significantly lesser extent.

Overall, the steering head region remains the most critical area of the structure and requires local reinforcement to ensure safety. Nevertheless, in terms of the average IRF values, the optimisation resulted in a 33 % reduction, demonstrating the beneficial effect of the modified geometry.

7.2.2 JUMP

In the baseline geometry, critical regions can be observed where the inverse reserve factor (IRF) exceeds 0.33 according to all applied failure criteria. As in the previous load case, the steering head is the most critical area due to stress concentrations, but additional exceedances also appear in the radius regions near the fuel tank inserts.

In the optimised geometry, values above the 0.33 threshold are still present in these areas, but to a much smaller extent. Nevertheless, both the steering head and the tank insert regions will require local reinforcement to ensure sufficient safety margins.

In terms of average IRF values, topology optimisation resulted in a 28 % reduction, confirming a substantial improvement in the overall structural response under this most demanding loading condition.

7.2.3 CORNERING

In the baseline geometry, a slight exceedance of the safety factor was observed in the steering head region, again due to stress concentrations in this critical area. Elevated values also appeared in the radius zones around the fuel tank inserts, but these did not reach critical levels.

In the optimised geometry, the same regions show increased IRF values; however, they remain below 0.2, and thus comfortably within the required safety margin.

From the perspective of the average IRF values, the optimised geometry achieved a 22 % reduction, confirming a noticeable improvement in the distribution of stresses even under this comparatively less demanding loading condition.

8 CONCLUSION

This dissertation focused on the optimisation of a motorcycle frame manufactured from carbon fibre reinforced polymers (CFRP), with the aim of verifying topology optimisation as a supporting tool for the design of bonded shell structures under real manufacturing constraints. Structural requirements were defined in terms of torsional, longitudinal, and lateral stiffness as well as safety under braking, jump landing, and cornering. A prototype monocoque frame, consisting of six composite and four aluminium parts, was manufactured using prepreg–autoclave technology, and material models were validated experimentally.

Topology optimisation was applied to the baseline geometry under three stiffness and three strength load cases, with a 40 % volume reduction constraint. The resulting design identified key load paths and weak regions, leading to targeted modifications: addition of an internal rib in the steering head, redesigned fuel tank mounts, conversion of outward flanges to internal lap joints, smoothing of geometry, reduction of part count, and simplified inserts and tooling.

Numerical analyses confirmed substantial improvements: torsional stiffness increased by 128 %, lateral by 140 %, and longitudinal by 67 %, with a 2 % mass reduction and lower stress concentrations. Despite these advances, the steering head remained critical, indicating the need for local reinforcement.

From a scientific perspective, the work confirmed that topology optimisation can be successfully applied to large CFRP shells when integrated with validated material models and manufacturing knowledge. From a practical perspective, the optimised design offers higher stiffness, lower weight, and simplified production, providing a cost-efficient and reproducible framework for lightweight structures. The study also highlighted the limitations of geometry-only optimisation, pointing to the necessity of laminate lay-up optimisation in future research.

In summary, the dissertation demonstrated that topology optimisation, when combined with technological constraints, is an effective approach for designing complex composite structures. The methodology and results are directly applicable to motorcycle engineering and transferable to broader transport and mechanical applications.

Tab. 10 Overall comparison – baseline vs optimised

Parameter	Non - optimised	Optimised	Percentual difference	design goal	Design goal achievement
Torsional stiffness [Nm $^{\circ -1}$]	2 376	5 405	+ 128 %	2 500	216 %
Longitudinal stiffness [N mm^{-1}]	403	671	+ 67 %	4 000	16.8 %
Lateral stiffness [N mm^{-1}]	480	1 150	+ 140 %	600	191.7 %
Braking IRF	0.0431	0.0288	- 33 %		
Jump IRF	0.109	0.0788	- 28 %		
Cornering IRF	0.0194	0.0152	- 22 %		
Mass [kg]	2.43	2.38	- 2 %		

REFERENCES

[1] VOGEL, Carl. *Build your own electric motorcycle*. New York: Mc Graw Hill, 2009. TAB Green guru guide. ISBN 978-0-07-162293-6.

[2] DARREN STILLWELL. *Motorcycle use in England*. 2016.

[3] CAPSONI, Doretta, Marcella BINI, Stefania FERRARI a Piercarlo MUSTARELLI. Lithium-Air Batteries Based on Carbon Nanomaterials. In: *Carbon Nanomaterials for Advanced Energy Systems* [online]. Hoboken, NJ: John Wiley & Sons, Inc, 2015, s. 385–405. Dostupné z: doi:10.1002/9781118980989.ch12

[4] NAQVI, Asad A., Awan ZAHOOR, Asif Ahmed SHAIKH, Faaz Ahmed BUTT, Faizan RAZA a Inam Ul AHAD. Aprotic lithium air batteries with oxygen-selective membranes. *Materials for Renewable and Sustainable Energy* [online]. 2022, **11**(1), 33–46. ISSN 2194-1459. Dostupné z: doi:10.1007/s40243-021-00205-w

[5] ZHU, Kunlei, Chao WANG, Zixiang CHI, Fei KE, Yang YANG, Anbang WANG, Weikun WANG a Lixiao MIAO. How Far Away Are Lithium-Sulfur Batteries From Commercialization? *Frontiers in Energy Research* [online]. 2019, **7**. ISSN 2296-598X. Dostupné z: doi:10.3389/fenrg.2019.00123

[6] MSR ENGINES S.R.O. *Interní analýza Hybrid X*. 2018.

[7] ZÁHORSKÝ, Lukáš. *Zelená paliva pro malé spalovací motory*. B.m.: Vysoké učení technické v Brně. Fakulta strojního inženýrství. 2023

[8] RITCHIE, H., M. ROSER a P. ROSADO. Energy. *Our world in Data* [online]. 2022 [vid. 2023-08-30]. Dostupné z: https://ourworldindata.org/energy

[9] LI, Yanmei, Ningning HA a Tingting LI. Research on Carbon Emissions of Electric Vehicles throughout the Life Cycle Assessment Taking into Vehicle Weight and Grid Mix Composition. *Energies* [online]. 2019, **12**(19), 3612. ISSN 1996-1073. Dostupné z: doi:10.3390/en12193612

[10] CARRANZA, Gerson, Martzel DO NASCIMIENTO, Josep FANALS, Josep FEBRER a César VALDERRAMA. Life cycle assessment and economic analysis of the electric motorcycle in the city of Barcelona and the impact on air pollution. *Science of The Total Environment* [online]. 2022, **821**, 153419. ISSN 00489697. Dostupné z: doi:10.1016/j.scitotenv.2022.153419

[11] ZHU, L., N. LI a P.R.N. CHILDS. Light-weighting in aerospace component and system design. *Propulsion and Power Research* [online]. 2018, **7**(2), 103–119. ISSN 2212540X. Dostupné z: doi:10.1016/j.jppr.2018.04.001

[12] HARRIS, Charles E., James H. STARNES a Mark J. SHUART. Design and Manufacturing of Aerospace Composite Structures, State-of-the-Art Assessment. *Journal of Aircraft* [online]. 2002, **39**(4), 545–560. ISSN 0021-8669. Dostupné z: doi:10.2514/2.2992

[13] ZHANG, Wen a Jun XU. Advanced lightweight materials for Automobiles: A review. *Materials & Design* [online]. 2022, **221**, 110994. ISSN 02641275. Dostupné z: doi:10.1016/j.matdes.2022.110994

[14] GUPTA, M. K. a R. K. SRIVASTAVA. Mechanical Properties of Hybrid Fibers-Reinforced Polymer Composite: A Review. *Polymer-Plastics Technology and Engineering* [online]. 2016, **55**(6), 626–642. ISSN 0360-2559. Dostupné z: doi:10.1080/03602559.2015.1098694

[15] NOVUS. Novus bike. *Novus GmbH* [online]. 2023 [vid. 2023-08-17]. Dostupné z: https://novusbike.com/bike-2/

[16] CAKE. *Cake bukk* [online]. 2023 [vid. 2023-08-28]. Dostupné z: https://ridecake.com/en/p/bukk

[17] ZHANG, Haoqi, Shuai WANG, Ka ZHANG, Jiang WU, Aonan LI, Jie LIU a Dongmin YANG. 3D printing of continuous carbon fibre reinforced polymer composites with optimised structural topology and fibre orientation. *Composite Structures* [online]. 2023, **313**, 116914. ISSN 02638223. Dostupné z: doi:10.1016/j.compstruct.2023.116914

[18] CHEN, Yuan a Lin YE. Topological design for 3D-printing of carbon fibre reinforced composite structural parts. *Composites Science and Technology* [online]. 2021, **204**, 108644. ISSN 02663538. Dostupné z: doi:10.1016/j.compscitech.2020.108644

[19] SCHWINGEL, Johannes a Peter MIDDENDORF. Topological design using multivariate laminate stackings for tailored fiber placement. *Journal of Composite Materials* [online]. 2022, **56**(13), 2047–2061. ISSN 0021-9983. Dostupné z: doi:10.1177/00219983221085721

[20] SPICKENHEUER, A., M. SCHULZ, K. GLIESCHE a G. HEINRICH. Using tailored fibre placement technology for stress adapted design of composite structures. *Plastics, Rubber and Composites* [online]. 2008, **37**(5), 227–232. ISSN 1465-8011. Dostupné z: doi:10.1179/174328908X309448

[21] COPPOLA, Anthony M., Scott R HUELSKAMP, Caleb TANNER, Daniel RAPKING a Richard D RICCHI. Application of tailored fiber placement to fabricate automotive composite components with complex geometries. *Composite Structures* [online]. 2023, **313**, 116855. ISSN 02638223. Dostupné z: doi:10.1016/j.compstruct.2023.116855

[22] SUZUKI, Takuya, Shinya FUKUSHIGE a Mitsuyoshi TSUNORI. Load path visualization and fiber trajectory optimization for additive manufacturing of composites. *Additive Manufacturing* [online]. 2020, **31**, 100942. ISSN 22148604. Dostupné z: doi:10.1016/j.addma.2019.100942

[23] VDOVIN, D, Y LEVENKOV a V CHICHEKIN. Light frame design for quad bike using topology optimization. *IOP Conference Series: Materials Science and Engineering* [online]. 2019, **589**(1), 012026. ISSN 1757-8981. Dostupné z: doi:10.1088/1757-899X/589/1/012026

[24] VLK, František. *Teorie a konstrukce motocyklů. díl 2.* 1. vyd. Brno: Prof.Ing.František Vlk, DrSc., 2004. ISBN 80-239-1601-7.

[25] BRADTMILLER, B., Hodge, B., Kristensen, S., Mucher, M. *Anthropometric Survey of Federal Aviation Administration Technical Operations Personnel - 2006-2008* [online]. Yellow springs: OH: Anthrotech. 2008 [vid. 2025-08-30]. Dostupné z: https://hf.tc.faa.gov/hfds/download-hfds/hfds_pdfs/App_B_Tech_Ops_Anthropometrics.pdf

[26] COSSALTER, Vittore. *Motorcycle dynamics*. 2nd English ed. S.l.: Lulu], 2006. ISBN 978-1-4303-0861-4.

[27] VLK, František. *Teorie a konstrukce motocyklů. díl 1.* 1. vyd. Brno: Prof.Ing.František Vlk, DrSc., 2004. ISBN 80-239-1601-7.

[28] MÍŠA, J. *Interní dokumentace - dynamický model 1/2 motocyklu*. 2021.

[29] GREGOR, Lukáš. *Návrh výroby kompozitní kyvné vidlice*. B.m.: Vysoké učení technické v Brně. Fakulta strojního inženýrství. 2020

CURRICULUM VITAE

Name and surname: **Ing. Lukáš Gregor**

Education:

Brno University of Technology - Faculty of Mechanical Engineering

2020 – pres. Ph.D. in Manufacturing technology
Thesis title: "Optimisation of motorcycle frame from composite materials considering manufacturing technology"

Supervisor: doc. Ing. Jan Zouhar Ph.D.

2018 – 2020 Ing. in Manufacturing technology and industrial management
Thesis title: "Manufacturing concept of a composite swingarm"

Supervisor: Ing. Jan Zouhar Ph.D.

2014 - 2018 Bc. – Fundaments of mechanical engineering
Thesis title: "Design of composite chassis for formula student vehicle"

Supervisor: Ing. Michal Mališ Ph.D.

Teaching/supervising experience:

PhD student, BUT - Faculty of Mechanical Engineering (2020 – now)

- Delivering lecture on MSc – Optical deformation systems, Composites – manufacturing technology
- Delivering teaching sessions on MSc - Numerical Modelling and Rapid Prototyping
- Delivering teaching sessions on BSc – Machining Technology
- Supervising 6 BSc and 3 MSc theses

Abroad experience:

- **Short PhD stay**

  20.5 – 19.6 2024 - Montanuniversität Leoben, Processing of Composites and Design for Recycling department

Employment:

7/2023 – present	Brno University of Technology Faculty of mechanical engineering Assistant
9/2020 – 6/2023	MSR Engines s.r.o. – JETSURF Head of CFRP development
1/2019 – 1/2021	Freelance designer
	MCAE Systems s.r.o.
9/2018 – 12/2018	Technician for 3D optical deformation measurement
1/2018 – 8/2018	3D Optical Digitization Technician

Extracurricular activities:

2019 – 2023	Faculty of Mechanical Engineering Brno University of Technology Academic senate Chamber of students member
	Formula student team – TU Brno Racing
2018 – 2020	Consultant
2016 – 2018	Chassis and composite leader
2015 – 2016	Chassis engineer

Language:

- Czech – native
- English – professional working proficiency
- French – elementary proficiency
- German – elementary proficiency

ABSTRACT

This dissertation focuses on the optimisation of a motorcycle frame made of carbon-fibre reinforced polymers (CFRP). The objective is to validate a design methodology for lightweight and structurally efficient composite structures using topology optimisation, while simultaneously accounting for laminate manufacturability. Structural requirements were defined in terms of torsional, longitudinal, and lateral stiffness, as well as safety under critical operating conditions such as braking, jump landing, and cornering. The baseline frame, manufactured using prepreg–autoclave technology, was analysed, and a design space for topology optimisation was established. The optimisation results were subsequently incorporated into the structural design with the dual aim of preserving manufacturability and reducing the number of assembly parts. The optimised frame achieved a 128 % increase in torsional stiffness, a 140 % increase in lateral stiffness, and a 67 % increase in longitudinal stiffness, while simultaneously reducing critical stress concentrations and achieving a 2 % weight reduction with an unchanged laminate lay-up. The results demonstrate that the use of topology optimisation as a supporting tool in the design of composite structures represents an effective pathway for the development of lightweight yet structurally safe CFRP components.